Published for SISSA by Springer

Received: *August 4, 2025*
Accepted: *September 13, 2025*
Published: *October 15, 2025*

New avenues for the neutrino dipole portal exploration at the energy frontier

Natascia Vignaroli

Dipartimento di Matematica e Fisica, Università del Salento,
and Istituto Nazionale di Fisica Nucleare, Sezione di Lecce,
I-73100 Lecce, Italy

E-mail: natascia.vignaroli@unisalento.it

Abstract: We present a comprehensive and gauge-invariant study of the neutrino dipole portal at the energy frontier. Assuming negligible active-sterile mixing, we analyze sterile neutrino production via dimension-6 dipole operators coupling to the electroweak field strengths. The analysis incorporates both single- and double-gauge-boson effective interactions. We investigate novel collider signatures at the HL-LHC, the FCC-hh — studied here in this context for the first time — and a 10 TeV muon collider. Particular emphasis is placed on electroweak boson-initiated processes, which dominate in the high-mass regime above ∼1 TeV. At the muon collider, these VBF-like topologies enable production even when the dipole couples to non-muonic flavors, offering a unique and sensitive probe for different flavor scenarios. We derive sensitivity projections for various theoretical benchmarks, reaching dipole couplings down to $d_\gamma \sim 6 \times 10^{-7}\,\text{GeV}^{-1}$ at FCC-hh and $d_\gamma \sim 2 \times 10^{-7}\,\text{GeV}^{-1}$ at the muon collider.

Keywords: Neutrino Interactions, Specific BSM Phenomenology, Sterile or Heavy Neutrinos, Baryon/Lepton Number Violation

ArXiv ePrint: 2507.01130

https://doi.org/10.1007/JHEP10(2025)125

JHEP10(2025)125

Contents

1 Introduction **1**

2 Theoretical framework **3**
2.1 Sterile neutrino decays 4

3 Hadron colliders **5**
3.1 Sterile neutrino production at hadron colliders 6
3.2 The high-luminosity LHC 7
3.3 The FCC-hh 9

4 Muon collider **16**
4.1 Sterile neutrino production at a muon collider 16
4.2 Search strategies and sensitivity projections in VBF channels 20

5 Results and outlook **22**

1 Introduction

The observation of neutrino oscillations provides unambiguous evidence that neutrinos are massive, implying the existence of physics beyond the Standard Model (SM). A minimal extension involves the addition of gauge-singlet right-handed neutrinos, often referred to as *sterile neutrinos* (N), which can couple to the SM via Yukawa interactions with lepton doublets and the Higgs field. These interactions, together with Majorana mass terms for the sterile states, can generate active neutrino masses through the seesaw mechanism [1–4]. Furthermore, sterile neutrinos may play a key role in explaining the baryon asymmetry of the Universe through leptogenesis [5, 6].

In this framework, the sterile neutrinos acquire electroweak interactions suppressed by the active-sterile mixing angle $\theta \sim \sqrt{m_\nu/m_N}$, which becomes small for sterile neutrino masses above the electroweak scale. As a consequence, obtaining evidence for the existence of sterile neutrinos based on mixing-induced interactions is challenging in this mass regime. However, if additional interactions are present, sterile neutrinos may remain experimentally accessible even when the mixing is negligible.

Among the possible new interactions, the *neutrino dipole portal* offers an attractive minimal and phenomenologically rich alternative. This portal connects active and sterile neutrinos via effective operators involving the field-strength tensors of the SM electroweak gauge symmetry. These interactions can dominate over the mixing-induced ones in scenarios where the active-sterile mixing is strongly suppressed or vanishing [7]. In the electroweak broken phase, such dipole operators generate magnetic-type couplings to the photon, Z, and W bosons.

Previous studies have analyzed the phenomenology of the dipole portal in both low-energy and high-energy regimes. For sterile neutrinos with sub-GeV masses, strong bounds arise

JHEP10(2025)125

from astrophysical observations, beam-dump experiments, and rare-meson decays [7–9]. At higher masses, collider-based searches become relevant. Several analyses have considered sterile neutrino production and decay via the photon dipole interaction, both at the LHC and at lepton colliders such as LEP [10] or future e^+e^- facilities such as CEPC [11]. Projections for LHC in its high luminosity phase (HL-LHC) have also been derived using searches for long-lived particles with displaced tracks [10, 12–15] and prompt $N \to \gamma\nu$ decays [9].

It is essential to consider that a complete and consistent formulation of the dipole portal at collider energies requires the use of dimension-6 operators invariant under the full $\mathrm{SU}(2)_w \times \mathrm{U}(1)_Y$ SM gauge symmetry. After electroweak symmetry breaking, these operators generate correlated dipole couplings to the γ, Z, and W bosons. This structure implies the existence of both neutral- and charged-current processes, and enhances the variety of possible collider signatures. Notably, charged-current channels such as $N \to W\ell$ can lead to clean leptonic final states, and radiation of electroweak bosons from the initial state becomes increasingly important at high energies. These features have recently been explored at a future muon collider [16, 17].

In this work, we present a *comprehensive and fully gauge-invariant analysis* of the neutrino-dipole portal at collider experiments, including not only the usual single-gauge-boson effective interactions, but also *genuine two-boson terms* that arise from the $\mathrm{SU}(2)_w$-invariant operator and are necessary for a correct treatment of neutrino-dipole portal processes at high energy. We assume a sterile neutrino with negligible active-sterile mixing and dominant dipole-mediated interactions.

The analysis covers different collider scenarios. We will start by exploring the reach of the upcoming High-Luminosity LHC (HL-LHC) program, for which we will investigate the range $m_N \gtrsim 100\,\mathrm{GeV}$, focusing in particular on the decays $N \to Wl$. We will then consider experiments at the energy frontier, in particular those supported by the recent European and US strategies for particle physics: a future circular collider (FCC) [18, 19] and a futuristic muon collider [20]. *For the first time, we will investigate the sensitivity of the FCC-hh* [21] and reconsider the sensitivity of a muon collider, recently explored in [16, 17]. The latter have shown that a muon collider would reach expected sensitivities of the order $\mathcal{O}(10^{-7})\,\mathrm{GeV}^{-1}$, which would be the best ever achieved in the region $m_N \gtrsim 1\,\mathrm{TeV}$. The sensitivity of future colliders to SM neutrino-dipole moments has instead been recently analyzed in [22].

A key focus of the present work is the role of electroweak boson radiation from the initial state, which gives rise to *sterile neutrino production via* scattering or fusion of weak bosons, which we concisely dub *vector-boson-fusion (VBF)*. Although VBF channels have not been systematically analyzed in the context of the dipole portal (a recent study [23] has shown their potential for the search for heavy Majorana neutrinos at muon colliders in the presence of significant mixing with the SM), we demonstrate that they provide very high sensitivity at high energies and large sterile neutrino masses. In particular, we present the *first dedicated analysis of these production modes at a muon collider*, showing that they allow sterile neutrinos to be efficiently produced *even when the dipole operator couples to flavors other than the muon.*

The remainder of the paper is structured as follows. In section 2, we introduce the theoretical framework, including the relevant gauge-invariant effective operators and their low-energy projections. After discussing sterile neutrino decay modes 2.1, in section 3 we present the collider analysis for hadronic machines: we will first discuss production channels (section 3.1) and then we will evaluate the sensitivity reach at the HL-LHC (section 3.2) and at the FCC-hh (section 3.3). Section 4 is devoted to muon collider analysis: we describe the dominant production channels in section 4.1, and present search strategies and sensitivity projections in VBF channels in section 4.2. Our conclusions are summarized in section 5.

2 Theoretical framework

In this study, we work under the hypothesis that neutrino-transition dipole moments constitute the dominant active-sterile portal interactions. We therefore assume negligible mixing between sterile and active neutrinos.

Dipole portal moments arise from the following 6-dimensional operators, which are generated by some new physics above the EW scale and which must respect the full $\mathrm{SU}(2)_w \times \mathrm{U}(1)_Y$ gauge symmetry of the SM:

$$\begin{aligned}\mathcal{L} &\supset \mathcal{C}_B^i \mathcal{O}_B^i + \mathcal{C}_W^i \mathcal{O}_W^i + \text{h.c.} \\ &= \mathcal{C}_B^i g' \bar{L}^i B_{\mu\nu} \tilde{H} \sigma^{\mu\nu} N + \mathcal{C}_W^i g \bar{L}^i W_{\mu\nu}^a \tau^a \tilde{H} \sigma^{\mu\nu} N + \text{h.c.}\,,\end{aligned} \tag{2.1}$$

where i is a flavor index, $g' = e\cos\theta_w$ and $g = e\sin\theta_w$ are the $\mathrm{U}(1)_Y$ and $\mathrm{SU}(2)_w$ gauge couplings, $\tau^a = \sigma^a/2$, with σ^a the Pauli matrices, $2\sigma^{\mu\nu} = i[\gamma^\mu, \gamma^\nu]$, $B_{\mu\nu}^a$ and $W_{\mu\nu}$ are the gauge field strengths of $\mathrm{U}(1)_Y$ and $\mathrm{SU}(2)_w$, $\tilde{H} = i\sigma^2 H^\star$ is the conjugate Higgs field, L is the lepton doublet and N the sterile neutrino, assumed to be of Majorana nature.

After spontaneous symmetry breaking of the Higgs, one obtains the following 5-dimensional effective interactions:

$$\begin{aligned}\mathcal{L} \supset\ & d_\gamma^i \bar{\nu}_L^i \sigma^{\mu\nu} N F_{\mu\nu} + d_Z^i \bar{\nu}_L^i \sigma^{\mu\nu} N Z_{\mu\nu} + d_W^i \bar{\ell}_L^i \sigma^{\mu\nu} N W_{\mu\nu}^- \\ & - d_W^i 2ig\, \bar{\ell}_L^i \sigma^{\mu\nu} N\, W_\mu^- (s_{\theta_w} A_\nu + c_{\theta_w} Z_\nu) + d_W^i \sqrt{2} ig\, \bar{\nu}_L^i \sigma^{\mu\nu} N\, W_\mu^- W_\nu^+ + \text{h.c.}\,,\end{aligned} \tag{2.2}$$

where $F_{\mu\nu}$ and $Z_{\mu\nu}$ are, respectively, the photon and the Z boson field strengths, s_{θ_w} (c_{θ_w}) shortly denotes the sin (cosine) of the Weinberg angle, and $W_{\mu\nu}^- \equiv \partial_\mu W_\nu^- - \partial_\nu W_\mu^-$. Note the presence of interaction terms between fermionic currents and two gauge bosons, which arise from the operator $\mathcal{O}_W$. These terms have been typically neglected in the previous literature [9, 16],[1] but play a crucial role in our study at the frontier of energy, since they are responsible for a dominant contribution to N production through VBF.

The dipole couplings in the broken phase are matched to the Wilson coefficients in the unbroken phase according to

$$\begin{aligned}d_\gamma^i &= \frac{ev}{\sqrt{2}} \left(\mathcal{C}_B^i + \frac{1}{2}\mathcal{C}_W^i \right) \\ d_W^i &= \frac{ev}{2s_{\theta_w}} \mathcal{C}_W^i \\ d_Z^i &= \frac{ev}{\sqrt{2}} \left(-\tan\theta_w \mathcal{C}_B^i + \frac{\cot\theta_w}{2} \mathcal{C}_W^i \right)\,,\end{aligned} \tag{2.3}$$

[1] I thank Vedran Brdar for clarifying that these terms were correctly included in the calculations performed in paper [17], even though they were not explicitly written in the initial version of their manuscript.

where $v = 246\,\text{GeV}$.[2] It is clear that the dipole couplings are not independent but intercorrelated through the coefficients $\mathcal{C}_B$ and $\mathcal{C}_W$. The correlation leads to an involved phenomenology that includes interference effects between various contributions. To properly examine the processes induced by a neutrino-dipole portal, we will, therefore, select theoretical benchmarks. In this study, we will specifically analyze the following:

(A) $\mathcal{C}_B = 0$ (B) $\mathcal{C}_W = \dfrac{2 s_{\theta_w} \tan\theta_w}{c_{\theta_w} - \sqrt{2}} \mathcal{C}_B \approx -\mathcal{C}_B \Leftrightarrow d_W = d_Z$

(C) $\mathcal{C}_W = 2\tan^2\theta_w \mathcal{C}_B \approx 0.57 \mathcal{C}_B \Leftrightarrow d_Z = 0$ (D) $\mathcal{C}_W = 0 \Leftrightarrow d_W = 0$

For simplicity, we will assume that $\mathcal{C}_B$ and $\mathcal{C}_W$ are real.[3] As will become clear in the following sections, these scenarios cover a wide range of possibilities for sterile neutrino phenomenology at colliders. The choice of these benchmarks is made by favoring a bottom-up perspective over a top-down approach, orienting ourselves towards the choice that gives rise to greater phenomenological differences. However, we stress that the study of ultraviolet (UV) completions of these benchmarks become obviously necessary to probe the regions of parameter space where the effective-field-theory (EFT) description loses validity, as we will show in our work. We defer the analysis of specific UV completions to future studies. For example, the analyzed benchmarks could be realized in leptoquark models, for suitable spectra and EW representations of the leptoquarks [8].

2.1 Sterile neutrino decays

The dipole interactions in eq. (2.2) allow for different production channels for the sterile neutrino at colliders, which will be examined in the next sections case by case depending on the type of collider, and lead to the three dominant N decays, $N \to \gamma\nu$, $N \to W\ell$, $N \to Z\nu$, with the following rates:

$$
\begin{aligned}
\Gamma_{N\to\nu^i\gamma} &= d_\gamma^{i\,2} \frac{m_N^3}{2\pi} \\
\Gamma_{N\to\ell^{i\pm}W^\mp} &= d_W^{i\,2} \frac{m_N^3}{2\pi} \left(1 - \frac{m_W^2}{m_N^2}\right)^2 \left(1 + \frac{m_W^2}{2m_N^2}\right) \\
\Gamma_{N\to\nu^i Z} &= d_Z^{i\,2} \frac{m_N^3}{2\pi} \left(1 - \frac{m_Z^2}{m_N^2}\right)^2 \left(1 + \frac{m_Z^2}{2m_N^2}\right) ,
\end{aligned}
\tag{2.4}
$$

where we have neglected the lepton masses, since in our study we are interested in a regime $m_N \gg m_\ell$. Dipole interactions with two gauge bosons (second line in eq. (2.2)) allow in principle also 3-body N decays. However, the corresponding rates are phase-space suppressed and negligible.

We show in figure 1 the N decay branching ratios (BRs) for the different benchmarks and for a specific flavor i. We can see that $N \to \gamma\nu$ is the dominant decay below the threshold for decays into $W\ell$, $m_N < m_W$, and for scenarios with smaller $\mathcal{C}_W$'s. Above the W mass, the

[2] We find a discrepancy of a factor $1/\sqrt{2}$ with the equation reported in version 1 of manuscript [17] for d_W (even taking into account the different definition of $\mathcal{C}_W$), while we agree with other previous literature [9, 16].

[3] In the more general case of complex coefficients, possible implications for CP violation are discussed for example in [24].

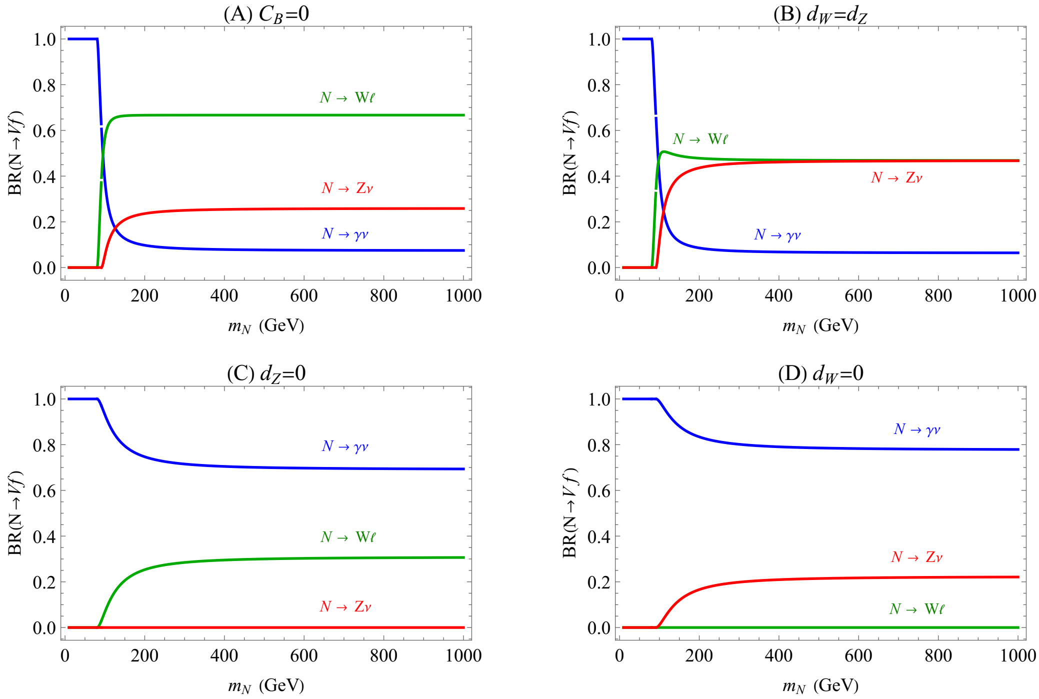

Figure 1. Decay branching ratios of the sterile neutrino, as function of its mass, for the four benchmarks: (A) $\mathcal{C}_B = 0$, (B) $d_W = d_Z$, (C) $d_Z = 0$ and (D) $d_W = 0$.

decay $N \to W^{\mp}\ell^{i\pm}$ has a zero BR, as expected, in the scenario (D) $d_W = 0$ but it becomes significant already in the scenario (C) $d_Z = 0$, while it is the dominant decay in the scenarios with larger $\mathcal{C}_W$'s. It should be noted that the detection of this leptonic decay at colliders would provide important additional information compared to the other decays into a boson plus a neutrino. In fact, by identifying the flavor of the emitted lepton, it would be possible to distinguish the specific flavor of the dipole operator responsible for the decay of N. For simplicity, in our analyses we will consider a flavor-universal scenario with $d^e = d^\mu = d^\tau$.

3 Hadron colliders

In this section, we perform an analysis of the projected sensitivities on the dipole-portal operator of future hadron colliders, the HL-LHC and the FCC-hh.

We rely on Monte Carlo simulations. Signal and background events are simulated with `MadGraph5` [25]. For the signal, the relevant interactions are implemented in `MadGraph5` using `Feynrules` [26]. The events are then passed to `Pythia8` [27] for showering. Jets are clustered with `Fastjet` [28] using an anti-k_t algorithm with cone size $R = 0.5$. To account for main detector effects, a smear is also applied to the 4-momenta of the jets, following the `Delphes` [29] default card. Moreover, when relevant, the missing transverse energy of each event is computed by including a Gaussian resolution $\sigma(E_T^{\text{miss}}) = 0.49\sqrt{\Sigma_i E_T^i}$, where $\Sigma_i E_T^i$ is the scalar sum of the transverse energies of all the reconstructed objects.

Statistical significance is assessed according to $\sigma \equiv N_S/\sqrt{N_S + N_B}$, where N_S (N_B) represents the number of signal (background) events.

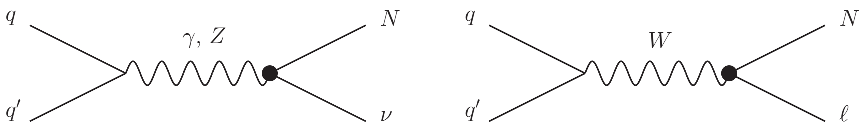

Figure 2. Feynman diagrams for the N production via s-channels at hadron colliders. Left diagram: $pp \to N\nu$ induced by the $\bar{\nu}\sigma^{\mu\nu}NF_{\mu\nu}$ or the $\bar{\nu}\sigma^{\mu\nu}NZ_{\mu\nu}$ dipole operator, whose amplitude is proportional to the coupling d_γ or d_Z respectively. Right diagram: $pp \to N\ell$ induced by the $\bar{\ell}_L\sigma^{\mu\nu}NW_{\mu\nu}$ dipole operator and with amplitude proportional to d_W.

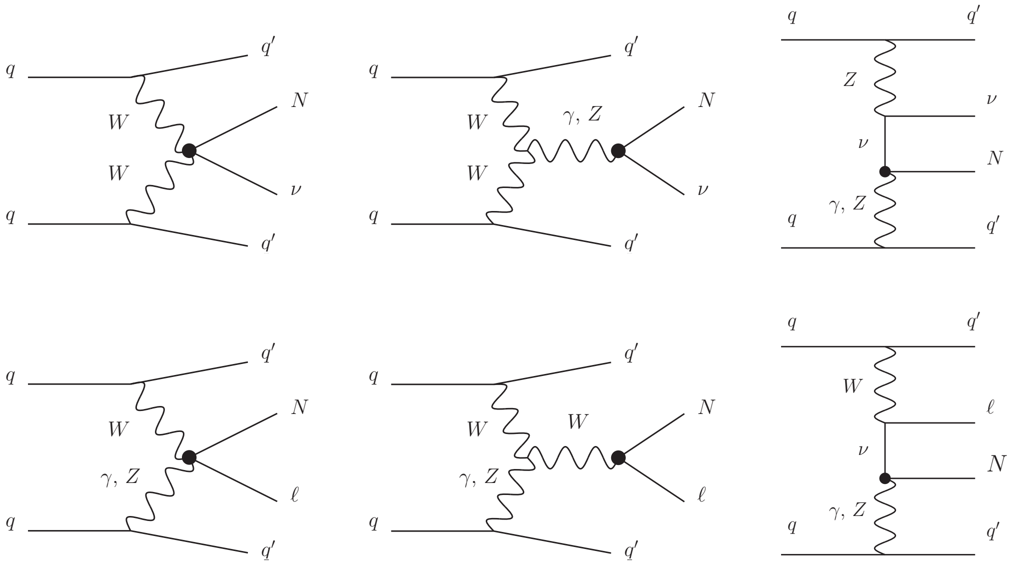

Figure 3. Representative Feynman diagrams for the production of N via VBF at hadron colliders. Upper diagrams: VBF N production in association with a neutrino. Lower diagrams: VBF N production in association with a lepton. The leftmost diagrams in the figure are generated by two-bosons effective interactions induced by the expansion of the dipole operator $\mathcal{O}_W$ (second line in eq. (2.2)) and have amplitudes proportional to d_W. The other diagrams are controlled by single-boson effective interactions induced by $\bar{\nu}_L\sigma^{\mu\nu}NF_{\mu\nu}$, $\bar{\nu}_L\sigma^{\mu\nu}NZ_{\mu\nu}$ or $\bar{\ell}_L\sigma^{\mu\nu}NW_{\mu\nu}$ and with amplitudes proportional to d_γ, d_Z or d_W respectively.

3.1 Sterile neutrino production at hadron colliders

Sterile neutrino production at hadron colliders can occur through two main mechanisms. The first category, as shown in figure 2, is production through s-channel exchange of neutral gauge bosons γ, Z, leading to processes $pp \to N\nu$, or via the charged boson W, leading to the N associated production with a lepton, $pp \to N\ell$. These processes are mediated by dipole operators with single-boson effective interactions (first line in eq. (2.2)) and have amplitudes proportional to the couplings d_γ, d_Z and d_W, respectively. The second category of processes, which, as we will see, is particularly relevant at higher energies, consists of the production of N by VBF, shown in figure 3. Both the production of N accompanied by a neutrino and that accompanied by a lepton are possible. These VBF processes result from the interplay of several different contributions, where the N production can be mediated by single-boson

JHEP10(2025)125

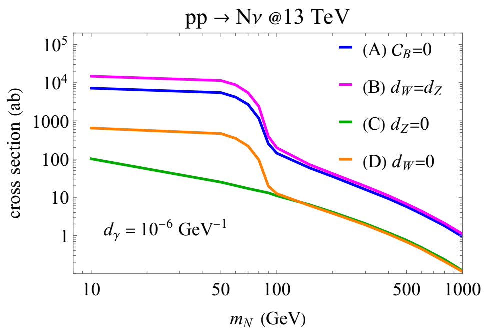

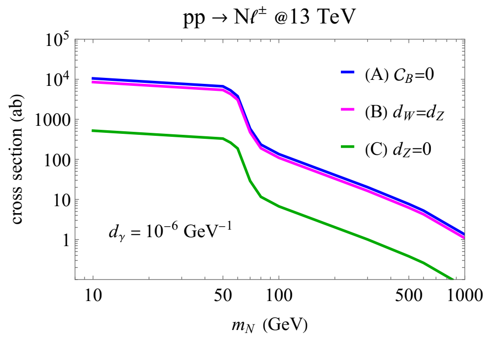

Figure 4. Cross section for the N production associated with a neutrino (left) and with a lepton, either a muon or an electron (right) at the HL-LHC for the different theoretical scenarios (A)-(D). Cross sections are shown for a reference value $d_\gamma = 10^{-6}\,\mathrm{GeV}^{-1}$.

effective interactions, induced by the operators $\bar{\nu}_L\sigma^{\mu\nu}NF_{\mu\nu}$, $\bar{\nu}_L\sigma^{\mu\nu}NZ_{\mu\nu}$ or $\bar{\ell}_L\sigma^{\mu\nu}NW_{\mu\nu}$, or by two-bosons effective interactions induced by the operator $\mathcal{O}_W$ (second line in eq. (2.2)). It is clear that to correctly evaluate N production via VBF, preserving gauge invariance, it is necessary to include all possible contributions. In particular, the effective interactions with two gauge bosons resulting from the expansion of the operator $\mathcal{O}_W$ cannot be neglected.

We remark some aspects of the N production at hadron colliders. N production can occur for any flavor of the dipole operator. As already specified, in the following analysis we will consider a universal flavor scenario. In the case of the N associated production with a lepton, the flavor of this lepton will be the same as that of the operator. By tagging its flavor it is therefore possible to extract information on the flavor of the dipole operator that allows the production of N. For simplicity, we will focus on processes with only electrons or muons, neglecting taus. Although, once the tau decays are properly analyzed, we expect similar sensitivities for the tau-flavored dipole operator.

3.2 The high-luminosity LHC

We start by evaluating the future sensitivities on d_γ of the HL-LHC. Conservatively, we consider a collision energy of 13 TeV and a final collected integrated luminosity of 3 ab^{-1}. The main N production at the HL-LHC is through s channels. N production through VBF would be possible in principle, but is subleading and negligible at the HL-LHC collision energy. We show in figure 4 the cross section for the N production at the HL-LHC in the different theoretical benchmarks.

Processes with subsequent decays $N \to \gamma\nu$ have already been analyzed in other studies [9, 17], which find sensitivities of the order of $d_\gamma \sim 3 \times 10^{-5}\,\mathrm{GeV}^{-1}$ in scenario (D) $d_W = 0$. In our analysis, we instead want to consider the decay $N \to W\ell$ in the remaining scenarios with $d_W \neq 0$. As already highlighted, this channel has the advantage of allowing the detection of the flavor related to the dipole operator responsible for the decay of N. We will consider in particular the production by s-channel W exchange, which combined with the leptonic decay of N leads to the following possible final states:

$$pp \to N\ell^{i\,\pm} \to W^\pm\ell^{j\,\mp}\ell^{i\,\pm}\,,\; W^\mp\ell^{j\,\pm}\ell^{i\,\pm}\,(\mathrm{SSD}) \tag{3.1}$$

we will then focus on events with hadronically decaying W's and with $\ell \equiv e, \mu$.

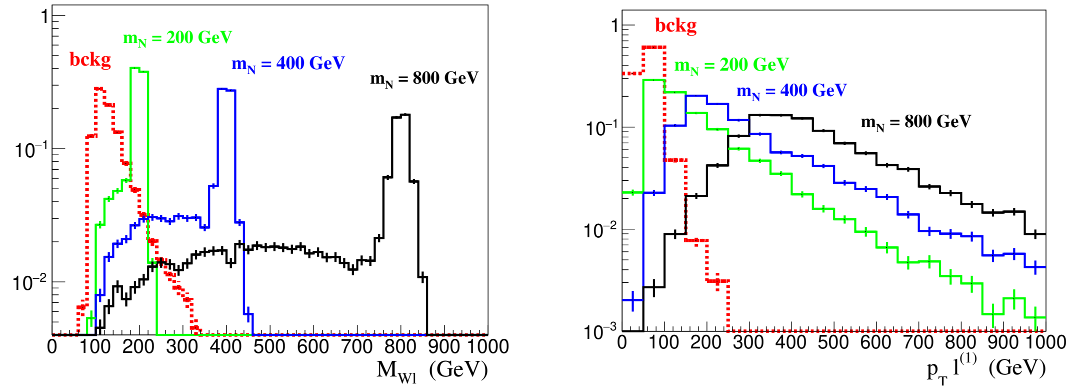

Figure 5. Distributions normalized to unit area for the $pp \to W_h^{\mp}\ell^{\pm}\ell^{\pm}$ neutrino dipole-portal signal with different N masses and for the SM background. Left plot: invariant mass of the system consisting of the hadronically decaying W and the nearest (in ΔR) lepton. Right plot: transverse momentum distribution of the p_T-leading lepton.

Notice that if the flavor of the N production operator is different from the one in the N decay ($i \neq j$), we will have two leptons with different flavors in the final state. Moreover, the two leptons will be kinematically different and thus distinguishable. Also note that, due to the Majorana nature of N, half of the decays will occur in two leptons with the same charge. Therefore, the process we will analyze could allow us to obtain multiple information: the chance of detecting and distinguishing the flavors of possibly different dipole operators responsible for the production and decay of N, the possibility of establishing the Majorana nature of the heavy neutrino.

We then focus on the final state with same-sign dileptons $W_h^{\mp}\ell^{\pm}\ell^{\pm}$ (SSD), which enjoys a rather low background, mainly given by $Z_\ell(\gamma_\ell^\star)$+jets and $Z_\ell(\gamma_\ell^\star)V_h$ events ($V_h \equiv W_h, Z_h$), where the charge of one of the leptons from $Z(\gamma^\star)$ decays is misidentified.[4] Additional background components are given by events with two gauge bosons decaying into leptons accompanied by jets, $W_\ell^{\pm}W_\ell^{\pm}(W_\ell^{\pm}Z_\ell)$+jets, and by the production of three gauge bosons, two of which decay leptonically and the other hadronically, $W_\ell^{\pm}W_\ell^{\pm}(W_\ell^{\pm}Z_\ell)V_h$. We require exactly two leptons with the same charge and at least two jets in the final state with transverse momenta $p_T > 20\,\text{GeV}$ and emitted in the central region, $|\eta| < 2.5$. We also require a minimal separation $\Delta R(\ell, j) > 0.4$ between the tagged jets and the leptons. For the signal, the two leading-p_T jets correctly reconstruct W_h. To reduce the background components $Z_\ell(\gamma_\ell^\star)$+jets and $W_\ell W_\ell(W_\ell Z_\ell)$+jets we apply the following condition on the invariant mass of the two leading-p_T jets: $M_{jj} \in [60\,\text{GeV},\, 90\,\text{GeV}]$. To reduce background sources from lepton charge misidentification, in particular Z_ℓ+jets, we apply a cut on the invariant mass of the two leptons: $M_{\ell^{(1)}\ell^{(2)}} > 100\,\text{GeV}$. After these acceptance criteria, the background is overall at the level of 7.9 fb.

We apply the following simple strategy to further reduce the background and identify the signal. The lepton resulting from the decay of N is for the vast majority of signal events the one closest to W_h, that is, the one with the smallest separation $\Delta R = \sqrt{\Delta\phi^2 + \Delta\eta^2}$

[4]We consider a misidentification rate of 0.1% [30].

JHEP10(2025)125

m_N in GeV	[150, 300)	[300, 500)	≥ 500
cuts in GeV	$p_T\ell^{(1)} > 50$, $M_{W_h\ell} > 100$	$p_T\ell^{(1)} > 100$, $M_{W_h\ell} > 200$	$p_T\ell^{(1)} > 150$, $M_{W_h\ell} > 400$
Bckg cross sec.	5.7 fb	0.65 fb	0.097 fb

Table 1. Set of cuts applied in signal selection for the different range of N masses at the HL-LHC. The background cross section after cuts is also reported.

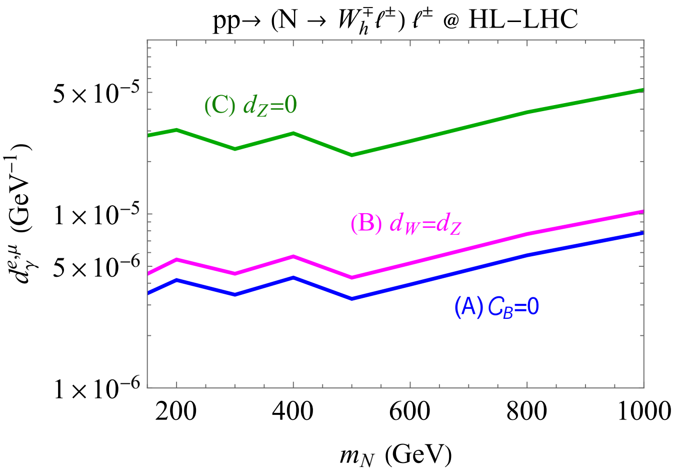

Figure 6. HL-LHC 2-σ sensitivities to the sterile neutrino dipole portal operator in the channel $pp \to W_h^{\mp}\ell^{\pm}\ell^{\pm}$ for the different theoretical benchmarks (A)-(C). A flavor-universal scenario $d_\gamma^e = d_\gamma^\mu = d_\gamma^\tau$ is assumed.

from W_h. In this way we can distinguish the lepton emitted in the decay of N from the one produced with it in association, and we can reconstruct quite well, as shown in figure 5, the sterile neutrino, starting from the invariant mass of its decay products: the W_h and the lepton just identified, $M_{W_h\ell}$. Moreover, for the range of N masses we are considering, the decay products are generally more energetic than for the background (figure 5). We can then further attenuate the background by applying a cut in the transverse momentum of the leading-p_T lepton. We then apply, depending on the mass of N, the three sets of cuts shown in table 1. We choose these cuts such that the signal with the lightest N, for each set, has an efficiency of at least 80%.

After the final selection, we find the 2σ sensitivities to the neutrino dipole portal operator shown in figure 6. We recall that since we focused on electrons or muons in the final state in a flavor-universal scenario, our analysis is equally sensitive to muonic and electronic flavors, $d_\gamma^{e,\mu}$. We can observe that the sensitivities in scenario (C) $d_Z = 0$ are similar to those estimated in the literature for scenario (D) $d_W = 0$, considering the decay channel $N \to \gamma\nu$. In the remaining benchmarks (B) $d_W = d_Z$ and (A) $\mathcal{C}_B = 0$ the sensitivities are significantly better, up to one order of magnitude, reaching values $d_\gamma \sim 3 \times 10^{-6}\,\text{GeV}^{-1}$.

3.3 The FCC-hh

We investigate now the sensitivity to the neutrino dipole portal of the future circular collider FCC-hh, with a nominal collision energy of 100 TeV. We assume an integrated collected luminosity of 30 ab^{-1}, based on the expected machine performances [21].

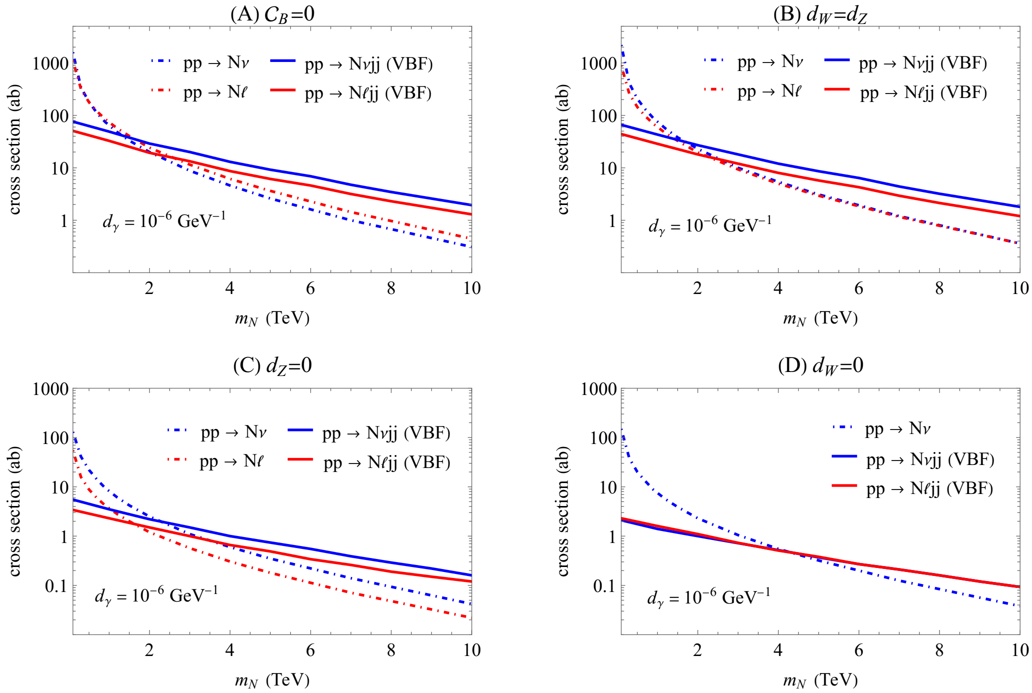

Figure 7. Cross section for the N production at the FCC-hh in the different theoretical benchmarks and channels: associated production with a neutrino (blue curves) or with a lepton (red curves) via s channels (dot-dashed curves) or through VBF (continuous curves). Cross sections are shown for a reference value $d_\gamma = 10^{-6}\,\mathrm{GeV}^{-1}$.

The scenario for sterile neutrino production changes significantly with the increasing of energy from the HL-LHC case, and we expect, in particular, an enhancement of the VBF production mechanisms. This is a general feature of future collider experiments at the energy frontier such as FCC-hh or the muon collider, which has been already emphasized in the literature (see for example [31–35]).

We show in figure 7 cross section values for the production of N in the different channels, the associated production with a neutrino or with a lepton through s channels or VBF, and for the theoretical benchmarks (A)-(D). We apply minimal requirements on the lepton in the associated production ℓN: $p_T > 20\,\mathrm{GeV}$, $|\eta| < 2.5$ and on the jets emitted in VBF processes: $p_T > 20\,\mathrm{GeV}$, $|\eta| < 5$. We can observe that VBF becomes significant for $m_N \gtrsim 1\,\mathrm{TeV}$ and is the leading production mechanism for the heavier sterile neutrinos. VBF is more significant for the theoretical scenarios with larger values of $\mathcal{C}_W$. This is expected due to the dominant role that the dipole operator $\mathcal{O}_W$ plays in VBF processes. For lighter N's, s-channel production is dominant, but the corresponding cross sections undergo a rapid decline as m_N increases. Given these considerations, we will analyze s channels, and, for the heavier N's, with masses greater than 1 TeV, we will also study the VBF processes.

s-channel

For the investigation in the s channels, in particular, we retrace the analysis performed for the HL-LHC in the **SSD** channel $pp \to W_h^\pm \ell^\mp \ell^\mp$. The main difference is a significant

JHEP10(2025)125

m_N in GeV	[150, 300)	[300, 500)	[500, 1000)	1000
cuts in GeV ($p_T\ell^{(1)}$, $M_{W_h\ell}$)	>50 , >100	>100 , >200	>150 , >400	>200 , >900
Bckg cross sec.	78 fb	13 fb	2.2 fb	0.092 fb

Table 2. Set of cuts applied in signal selection in the s-channel $W_h^{\pm}\ell^{\mp}\ell^{\mp}$ for the different range of N masses at the FCC-hh. The background cross section after cuts is also reported.

increase in the boost of the final products at FCC-hh. W_h thus decays into a single fat-jet for the vast majority (more than 80%) of signal events with $m_N \geq 1\,\text{TeV}$. For these heavier N's we therefore identify the W_h of the signal with the leading-p_T jet in the final state and we require its invariant mass to lie in the interval [60 GeV, 90 GeV].[5] For the signal with $m_N < 1\,\text{TeV}$ the W_h is reconstructed from the leading- and the second leading-p_T jets. To attenuate background sources from misidentified lepton charges, we also apply the condition $M_{\ell^{(1)}\ell^{(2)}} > 100\,\text{GeV}$. The sterile neutrino can be efficiently reconstructed with the same strategy outlined in the previous section for HL-LHC, by considering the W_h and the nearest lepton. We also apply the same set of cuts for the lighter N's. Note that this is a conservative choice because, again due to the greater boost, the leading-p_T lepton of the signal is more energetic (generally 20% more) than in the case of HL-LHC and therefore even more stringent cuts could be applied. The background, again dominantly given by $Z_\ell(\gamma_\ell^\star)$+jets and $Z_\ell(\gamma_\ell^\star)V_h$ ($V_h \equiv W_h, Z_h$) events with misidentified lepton charges and by $W_\ell^{\pm}W_\ell^{\pm}(W_\ell^{\pm}Z_\ell)$+jets and $W_\ell^{\pm}W_\ell^{\pm}(W_\ell^{\pm}Z_\ell)V_h$, has a total cross section of 102 fb after acceptance requirements. The total background cross section reduces as shown in table 2 after each set of cuts. Additionally, for N heavier than 1 TeV we will apply the cut: $M_{W_h\ell} > 90\% \cdot m_N$.

In scenario (D) $d_W = 0$ the SSD channel considered sofar is absent, but we can derive a rough estimate of the FCC-hh sensitivity starting from the HL-LHC estimate made in the literature considering the decay channel $N \to \nu\gamma$ [9, 17]. Based on a simple scaling of the signal and the dominant background cross sections, and taking into account the different integrated luminosities, we find sensitivities in the range of $d_\gamma \sim 6 \times 10^{-6}\,\text{GeV}^{-1}$ for the FCC-hh in the scenario $d_W = 0$ and $m_N \lesssim 1\,\text{TeV}$.

We will now outline signal selection strategies for **VBF processes**. Several VBF channels can be analyzed. Depending on N production and decay modes, we can list the following possible final states:

(i) $(N \to W^{\pm}\ell^{\mp})\nu jj \to W^{\pm}\ell^{\mp}jj + E^{\text{miss}}$

(ii) $(N \to W\ell)\ell jj \to W\ell\ell jj$ (SSD+OSD)

(iii) $(N \to \gamma\nu)\ell^{\pm}jj \to \gamma\ell^{\pm}jj + E^{\text{miss}}$

(iv) $(N \to \gamma\nu)\nu jj \to \gamma jj + E^{\text{miss}}$

(v) $(N \to Z\nu)\ell^{\pm}jj \to Z\ell^{\pm}jj + E^{\text{miss}}$

(vi) $(N \to Z\nu)\nu jj \to Zjj + E^{\text{miss}}$

where E^{miss} denotes the missing energy associated with neutrinos. Note that channel (ii) includes final states with dileptons of both opposite sign charges (OSD) and same sign (SSD). The latter arise from the Majorana nature of N.

[5] This requirement strongly reduces in particular the $Z_\ell(\gamma_\ell^\star)$+jets background component, for which the leading-p_T jet has generally an invariant mass lower than 60 GeV.

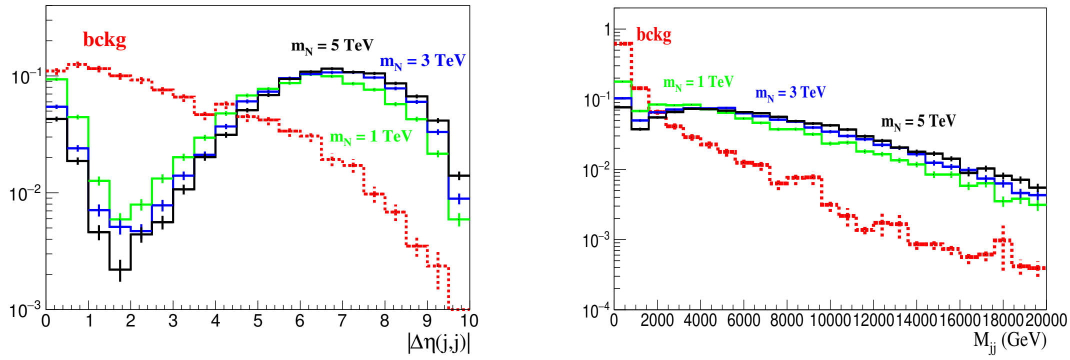

Figure 8. Distributions normalized to unit area for the $pp \to W_h^{\pm}\ell^{\mp}\ell^{\mp}jj$ VBF dipole-portal signal in scenario (A) $\mathcal{C}_B = 0$ with different N masses, and for the SM background. We plot the pseudorapidity separation of the two VBF jets (left plot) and their invariant mass (right plot).

An intertwined analysis of all these final states would be particularly interesting to extract multiple information and increase the sensitivity to the dipole portal operator. As already highlighted, channels (ii) and (iii) where N is produced in association with a lepton could allow, for example, the detection of the flavor of the dipole operator which induces N production. For effectiveness and concreteness, we focus in this study on some of the most interesting channels and defer a joint analysis to future investigations. Given the higher decay BRs and the possibility of reconstructing the sterile neutrino from its visible decay products, we will focus on channels (i) and (ii), with final hadronically decaying W's, for the theoretical scenarios (A) $\mathcal{C}_B = 0$ and (B) $d_W = d_Z$. In the analysis of channel (ii), we will focus in particular on the SSD final state, which enjoys a lower SM background. Due to the reduced or absent decay BRs in $W\ell$, for scenarios (C) $d_Z = 0$ and (D) $d_W = 0$ we will instead focus on the final state (iii), where the sterile neutrino decays into a neutrino plus a photon.

A common feature of these VBF channels, which we exploit to select the sterile neutrino signal from the background, is the peculiar kinematics of the two final jets. As a characteristic of VBF processes, these jets are emitted forward-backward at high rapidity and therefore have a separation $\Delta\eta$ generally much higher than for the background. The invariant mass of the two jets tends to be higher as well. We show in figure 8 the distributions $\Delta\eta(j,j)$ and M_{jj} in the illustrative case of signal (ii) for the theoretical scenario (A) $\mathcal{C}_B = 0$. Very similar distributions are obtained for the other VBF channels and theoretical benchmarks.

In all the VBF channels we will analyze, we will apply the following cuts on the VBF jets:

$$|\Delta\eta(j,j)| > 3\,, \quad M_{jj} > 500 \text{ GeV} \tag{3.2}$$

Another common feature is the fact that at FCC-hh, as already underlined, W_h decays into a single, central, high-p_T fat jet for the vast majority (more than 80%) of signal events with $m_N \geq 1$ TeV. The two jets emitted by VBF are instead softer (as well as generally emitted at higher rapidity). In the following analyses, W_h will therefore be identified with the leading-p_T jet of the final state, and we will require that its invariant mass is in the range 60–90 GeV. Other selection strategies are discussed channel by channel.

(i) $\mathbf{W_h^\pm \ell^\mp jj + E^{miss}}$

We require exactly one lepton with $p_T > 20\,\text{GeV}$ and $|\eta| < 2.5$ and at least three jets with $p_T > 20\,\text{GeV}$, $|\eta| < 5$ and separated from each other and from the lepton by $\Delta R(j,j), \Delta R(j,\ell) > 0.4$. The dominant background is given by $V_h W_\ell$+jets events, where the jets (at least two) are produced by QCD, or by EW interactions. This latter category includes the EW production of two gauge bosons, via VBF, and of three gauge bosons. An additional background component arises from W_ℓ+jets, with at least three QCD jets. The latter process has a cross section of about 10^4 pb after minimal acceptance cuts, which is, however, strongly reduced to the level of 10 pb, by imposing that the leading-p_T jet has an invariant mass between 60 and 90 GeV, so as to mimic the W_h of the signal. The cross sections, before selection, of the remaining $V_h W_\ell$+jets backgrounds are about 130 pb for the events with QCD jets and about 4.4 pb for the component with EW jets. As a first step of signal selection, we apply the VBF cuts in eq. (3.2). The total background cross section is then reduced to 23 pb, while more than 80% of the signal events are retained. In the second step, the sterile neutrino can be easily reconstructed, from the W_h and the lepton, and we can exploit the characteristic of the signal to emit energetic final states. We apply the cuts:

$$p_T\ell > 200\,\text{GeV}, \quad E_T^{\text{miss}} > 200\,\text{GeV}, \quad p_T W_h > 200\,\text{GeV}, \quad M_{W_h\ell} > 95\% \cdot m_N$$

The signal efficiency to these cuts (after passing the VBF selection) is greater than 90% while the background cross section is reduced to less than 61 fb.

(ii) $\mathbf{W_h^\pm \ell^\mp \ell^\mp jj}$ (SSD)

Given the low background, consisting of only reducible components, we analyze the SSD channel. We focus on a final state consisting of exactly two leptons with the same charge, and with $p_T > 20\,\text{GeV}$ and $|\eta| < 2.5$, and of at least three jets with $p_T > 20\,\text{GeV}$, $|\eta| < 5$, and separated from each other and from the leptons by $\Delta R(j,j), \Delta R(j,\ell) > 0.4$. The leading-$p_T$ jet, which is the W_h of the signal, must have an invariant mass in the range 60–90 GeV. Dominant background processes include $W_\ell^\pm W_\ell^\pm V_h$+jets, where the jets, at least two, are produced by QCD or EW interactions and $Z_\ell(\gamma_\ell^\star)$+($\geq 3$) jets or $Z_\ell(\gamma_\ell^\star)V_h$+($\geq 2$) jets events with misidentified lepton charges. The latter are strongly reduced by imposing the condition on the invariant mass of the two leptons: $M_{\ell^{(1)}\ell^{(2)}} > 100\,\text{GeV}$. $W_\ell^\pm W_\ell^\pm$+(≥ 3)jets is attenuated to a negligible level by the leading-p_T invariant mass condition. After acceptance requirements, the background cross section is overall 50 fb. Similarly to the case of the SSD signal in the s channel, the sterile neutrino can be efficiently reconstructed by considering the W_h and the nearest (with the smaller ΔR separation) lepton. The corresponding invariant mass distributions, $M_{W_h\ell}$, are shown in figure 9 for the signal with different N masses and for the background. We plot signal distributions for scenario (A). Very similar distributions are obtained in the theoretical benchmark (B).

In our analysis, we first apply the VBF cuts in eq. (3.2) and then refine the selection by applying the following conditions on the leading-p_T lepton and invariant mass of the reconstructed N:

$$p_T\ell^{(1)} > 200\,\text{GeV}, \quad M_{W_h\ell} > 90\% \cdot m_N$$

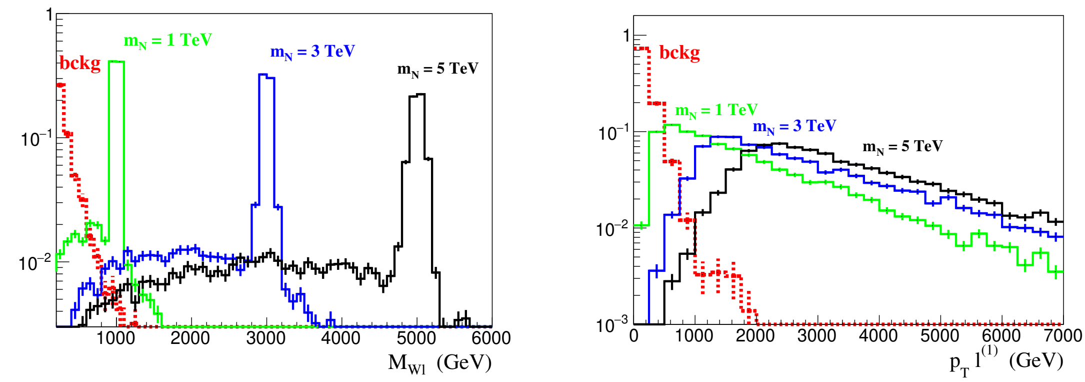

Figure 9. Distributions normalized to unit area for the $pp \to W_h^{\pm} \ell^{\mp} \ell^{\mp} jj$ VBF dipole-portal signal in scenario (A) $\mathcal{C}_B = 0$ with different N masses, and for the SM background. We plot the invariant mass of the system consisting of the W_h and the nearer lepton (left plot) and the transverse momentum of the leading-p_T lepton (right plot).

$p_T \ell^{(1)}$ distributions for signal and background are also shown in figure 9. Signal efficiencies for this selection are above 75%, while the background cross section is reduced to less than 0.7 fb.

(iii) $\ell^{\pm}\gamma$jj + E$^{\text{miss}}$

For the theoretical scenarios (C) and (D), we focus on the VBF N production associated with a lepton followed by the decays $N \to \gamma\nu$. The final state we analyze consists of one high energetic lepton, one high energetic photon, at least two jets, and large missing energy. The acceptance requirements are: $p_T > 20\,\text{GeV}$ for the transverse momenta of all the final state particles, $|\eta| < 2.5$ for the lepton and photon, and $|\eta| < 5$ for the jets. Photon, lepton and jets must be separated by $\Delta R > 0.4$. The leading SM background is given by $W_\ell \gamma$+jets events, where the jets (at least two) are produced by QCD or EW interactions. The latter include VBF $W\gamma$ production. After acceptance requirements, the background cross section is of 67 pb. As for the other VBF channels, we select our signal by first applying the VBF cuts in eq. (3.2) and then we refine the analysis by exploiting the kinematic characteristics of the signal (cf. figure 10). In particular, we apply the cuts:

$$p_T \ell > 200\,\text{GeV}, \quad p_T \gamma > 200\,\text{GeV}, \quad E_T^{\text{miss}} > 200\,\text{GeV}, \quad M_T(N) > 90\% \cdot m_N\,,$$

where $M_T(N)$ denotes the transverse mass of the sterile neutrino, which is defined as

$$M_T(N) \equiv \sqrt{2\, E_T^{\text{miss}}\, p_T \gamma\, \left(1 - \Delta\phi(E^{\text{miss}}, \gamma)/\pi\right)}\,.$$

Signal efficiencies to this selection are higher than 70%, while the background is reduced to less than 15 fb.

At the end of our analyses in the various channels we find the 2σ sensitivities of FCC-hh to the dipole operator d_γ shown in figure 11 for the different theoretical scenarios (A)-(D). The projected sensitivities equally refer to a muonic or electronic flavor[6] (we recall that we

[6]Possible differences due to different identification efficiencies of muons or electrons are negligible for our purposes.

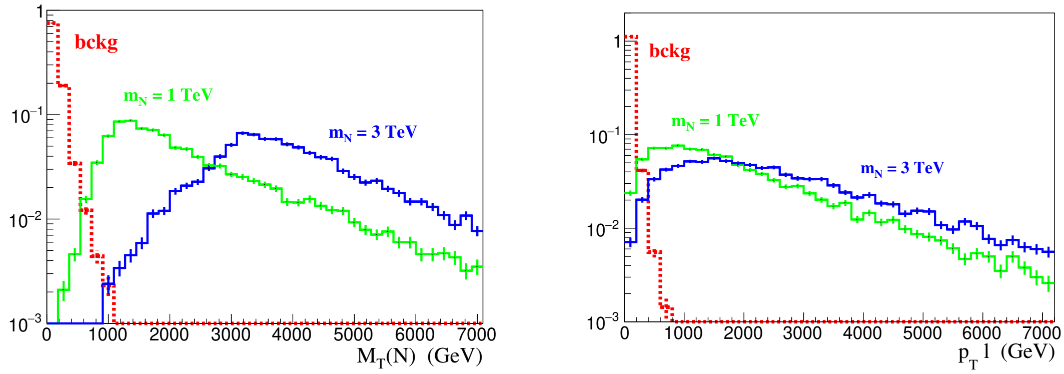

Figure 10. Distributions normalized to unit area for the $pp \to \ell^{\mp}\gamma jj + E^{\text{miss}}$ VBF dipole-portal signal in scenario (D) $d_W = 0$ with different N masses, and for the SM background. We plot the transverse mass of the sterile neutrino (left plot) and the transverse momentum of the lepton (right plot).

have assumed a universal flavor scenario). We show the sensitivities corresponding to each of the channels analyzed. In the case of the s channel for the benchmark (D), the reported sensitivity is the one extrapolated from the results of the recent literature [9, 17] considering $N \to \gamma\nu$ decays. The shaded regions in the upper right are indicative of a parameter space where the effective-field-theory description cannot be valid.

The EFT validity regime can be estimated in Naive-Dimensional-Analysis (NDA) by considering the following power counting for the Wilson coefficients, which are generated at loop level [7, 22]:

$$\mathcal{C}_{B,W} \approx \frac{g_\star^2}{16\pi^2 m_\star^2}\,, \tag{3.3}$$

where $m_\star$ is a typical mass in the UV physics which generates the operators $\mathcal{O}_{B,W}$ and $g_\star$ denotes a typical coupling between the sterile neutrino and the UV fields. We can set $m_\star \approx m_N$, using m_N to approximate the momentum transfer for the considered s-channel and VBF processes. In a strongly-coupled regime, $g_\star \sim 4\pi$, we therefore fall outside the EFT validity regime when the sterile neutrino mass is above the energy scale of the Wilson coefficients, namely $m_N \gtrsim \sqrt{\mathcal{C}_{B,W}^{-1}}$. Notice, however, that in a weakly-coupled theory, $g_\star \lesssim 1$, the constraints would be tighter and the EFT validity would already be lost for $m_N \gtrsim \sqrt{\mathcal{C}_{B,W}^{-1}}/4\pi$. In this scenario, the EFT would be invalid in most of the multi-TeV parameter space that would be explored at the energy frontier. The attractive implication is that the weakly-interacting regime would first emerge with the direct discovery at future colliders of new states from the UV physics. The interesting investigation of this situation is deferred to specific analyses in UV completed theories.

As figure 11 illustrates, the sensitivity of the s-channel $pp \to W_h^{\pm}\ell^{\mp}\ell^{\mp}$ is of the order of $5\times10^{-6}\,\text{GeV}^{-1}$ in scenario (C) and improves to values slightly below $1\times10^{-6}\,\text{GeV}^{-1}$ in benchmarks (A) and (B). For sterile neutrino masses greater than about 2 TeV, we can see how VBF channels offer the best opportunities to probe d_γ. For scenarios (C) and (D), the study of the channel $pp \to \ell^{\pm}\gamma jj + E^{\text{miss}}$ allows testing dipole operators of the order of $4\times10^{-6}\,\text{GeV}^{-1}$ up to masses m_N of about 5 and 3.5 TeV, respectively. The VBF channel $pp \to W_h^{\pm}\ell^{\mp}\ell^{\mp}jj$

JHEP10(2025)125

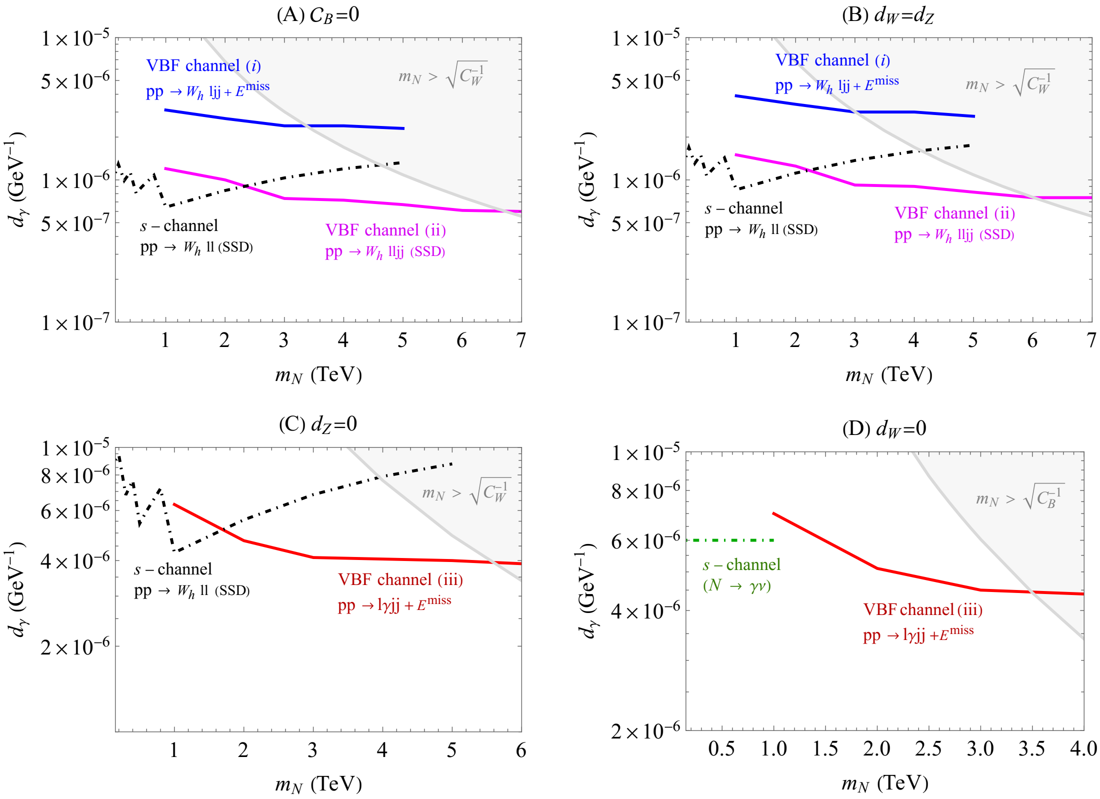

Figure 11. 2σ sensitivities of FCC-hh to the dipole operator d_γ for the various theoretical benchmarks considered and in the different analyzed channels.

presents the highest sensitivities, that reach d_γ of the order of 0-9$\times10^{-7}$ GeV^{-1} up to masses m_N of about 6 TeV for scenarios (A) and (B). Finally, as already underlined, it should be noted that the most efficient channels also offer the possibility of gaining information on the flavor of the dipole operator, which would be obtained by tagging the leptonic flavor.

4 Muon collider

We reconsider the sensitivity of the muon collider to the dipole portal, highlighting the importance of VBF heavy neutrino production channels that have been overlooked in recent studies [16, 17].

The singular advantage of VBF channels is that they allow significant N production at the muon collider even for flavors other than muonic. In addition, in the cases with $\mathcal{C}_W \neq 0$, we will show that it is necessary, in order to preserve EW gauge invariance and for a correct evaluation of the N production processes, to include all effective interaction terms, in particular those with two gauge bosons from the expansion of $\mathcal{O}_W$.

We will consider a muon collider with a collision energy $\sqrt{s}$ =10 TeV and an integrated luminosity of 10 ab^{-1}, which is expected to be collected at the end of a ∼5 year run [20].

4.1 Sterile neutrino production at a muon collider

The N production in a muon collider can proceed through several processes. The most relevant ones can be classified into three categories: the 2-2 process $\mu^+\mu^- \to N\nu$, 2-3 processes induced by the exchange in the t-channel of a gauge boson W, Z or γ, and the VBF production, which consists of 2-4 processes induced precisely by the exchange of two gauge bosons in the t-channel.

In more detail, the 2-2 $\mu^+\mu^- \to N\nu$ production process, shown in figure 12, can receive a contribution from the s-channel exchange of γ or Z bosons, induced by the dipole operators $\bar{\nu}\sigma^{\mu\nu}NZ_{\mu\nu}$ or $\bar{\nu}\sigma^{\mu\nu}NF_{\mu\nu}$, and a contribution from the t-channel exchange of a W, induced by $\bar{\ell}_L\sigma^{\mu\nu}NW_{\mu\nu}$. Note that while the s-channel production is flavor independent, the t-channel production is only possible for the muon flavor. Generally, the contribution to the t-channel cross section is dominant. We find that contribution from t-channel W exchange is about two orders of magnitude larger than s-channel ones in scenarios (A) and (B), and one order of magnitude in scenario (C). Obviously, the t-channel contribution is absent for scenario (D) $d_W = 0$.

The production in 2-3 processes is shown in figure 13. Production in both the neutral channels $\mu^+\mu^- \to N\gamma\nu, NZ\nu$ and the charged channel $\mu^+\mu^- \to NW\mu$ is possible. Again, N production is only possible for the muonic flavor. Note that, except for the case $\mathcal{C}_W = 0$ ($d_W = 0$), there are two main contributions to 2-3 processes, the one induced by single-boson effective interactions (left diagrams in figure 13) and the one induced by effective interactions with two gauge bosons, generated by the expansion of the operator $\mathcal{O}_W$ (right diagrams in figure 13). Both of these contributions must be included for a correct gauge-invariant treatment. In fact, if two-boson effective interaction diagrams are neglected, the evaluation of 2-3 processes (with the exception of the benchmark (D) $d_W = 0$) shows, as an effect of the violation of the EW gauge invariance, an apparent but not consistent increase in the respective cross sections.

Finally, N can be produced, similar to what was previously considered in hadron colliders, via VBF. Such production is possible for any flavor, not just the muon. The 2-4 VBF processes, of which we show representative diagrams in figure 14, consist of both neutral $\mu^+\mu^- \to N\nu\nu_\mu\bar{\nu}_\mu$ and charged $\mu^+\mu^- \to N\ell\mu\nu$ channels. Note that the latter also include $\mu^+\mu^- \to N\nu\mu^+\mu^-$ events, generated from the scattering of two neutral bosons (last diagram in figure 14).[7] VBF production at a muon collider depends on a delicate balance between numerous contributions involving single- and double-boson effective vertices and different dipole operators. Also in this case it is crucial to include all possible contributions in order to correctly evaluate, in a gauge-invariant way, the processes.

We show in figure 15 cross sections for the N production in the different processes and theoretical benchmarks. We consider hadronically decayed bosons in 2-3 processes $\mu^+\mu^- \to N\mu W_h$, $N\nu Z_h$. We find that flavor-independent VBF production is relevant in all theoretical scenarios considered and generally exhibits higher cross sections, as expected, in scenarios with higher $\mathcal{C}_W$ values. The lepton-associated VBF production $\mu^+\mu^- \to N\ell\mu\nu$ is particularly notable, constituting the production channel with the highest cross section, after $\mu^+\mu^- \to NW_h\mu$, in scenarios (B), (C) and (D).

[7]This is an important difference with the case of VBF production at hadron colliders, where N production accompanied by a lepton can only occur by WV fusion ($V \equiv Z, \gamma$), while VZ scattering contributes to the lepton-free final state. For this reason, at the muon collider the "charged" VBF production is generally more relevant than the "neutral" one.

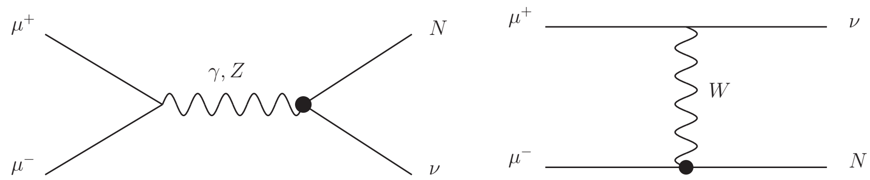

Figure 12. Feynman diagrams for the N production at a muon collider in *2-2 processes*. Left diagram: s-channel production induced by the $\bar{\nu}\sigma^{\mu\nu}NF_{\mu\nu}$ or the $\bar{\nu}\sigma^{\mu\nu}NZ_{\mu\nu}$ dipole operator, whose amplitudes are proportional to the coupling d_γ or d_Z respectively. Right diagram: t-channel production induced by the $\bar{\ell}_L\sigma^{\mu\nu}NW_{\mu\nu}$ dipole operator and with amplitude proportional to d_W.

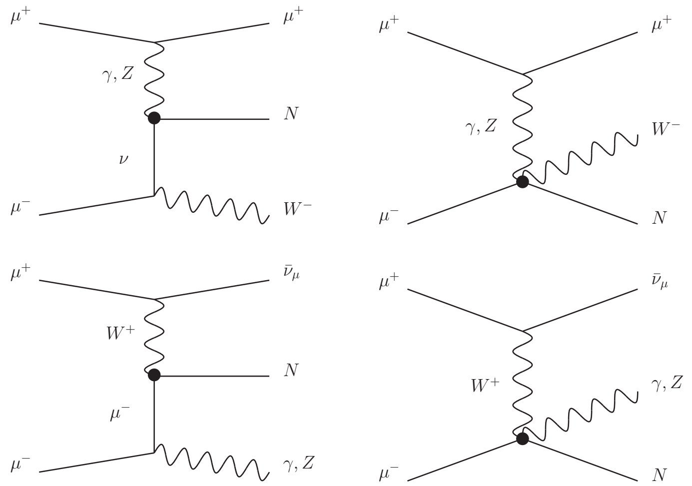

Figure 13. Leading Feynman diagrams for the N production at a muon collider in *2-3 processes*. Upper diagrams: $\mu^+\mu^- \to NW\mu$. Lower diagrams: $\mu^+\mu^- \to N\gamma\nu, NZ\nu$. The diagrams on the left are generated by induced dipole effective interactions with a single boson (with couplings d_γ, d_Z or d_W, depending on the specific boson). The diagrams on the right are induced by effective interactions with two gauge bosons, emerging from the expansion of the dipole operator $\mathcal{O}_W$, with amplitudes proportional to d_W.

The 2-2 process is, with the exception of scenario (D), one of those with the highest cross section. The 2σ sensitivity to the $d_\gamma^{(\mu)}$ operator in this channel has been evaluated in [16, 17], obtaining values in the range 1-2 $\times 10^{-6}\,\text{GeV}^{-1}$ in scenario (C) $d_Z = 0$. In scenarios (B), (C), and (D), the 2-3 process $\mu^+\mu^- \to N\mu W_h$, has the highest cross section. In scenario (D), the 2σ sensitivity to the $d_\gamma^{(\mu)}$ operator in this channel evaluated in [16] is approximately $1 \times 10^{-7}\,\text{GeV}^{-1}$. For the other theoretical benchmarks, however, the channel sensitivity should be re-evaluated through a gauge-invariant treatment, which we defer to future studies. In the present work, we instead want to focus on flavor-independent VBF channels. Depending on the decays of N, we can distinguish the following final states:

(i) $(N \to W^\pm\ell^\mp)\nu\nu_\mu\bar{\nu}_\mu \to W^\pm\ell^\mp + E^{\text{miss}}$

(ii) $(N \to W\ell)\ell\mu\nu \to W\ell\ell\mu + E^{\text{miss}}$

(iii) $(N \to \gamma\nu)\ell^\pm\mu^\mp\nu \to \gamma\ell^\pm\mu^\mp + E^{\text{miss}}$

(iv) $(N \to \gamma\nu)\nu\nu_\mu\bar{\nu}_\mu \to \gamma + E^{\text{miss}}$

(v) $(N \to Z\nu)\nu\nu_\mu\bar{\nu}_\mu \to Z + E^{\text{miss}}$

(vi) $(N \to Z\nu)\ell^\pm\mu^\mp\nu \to Z\ell^\pm\mu^\mp + E^{\text{miss}}$

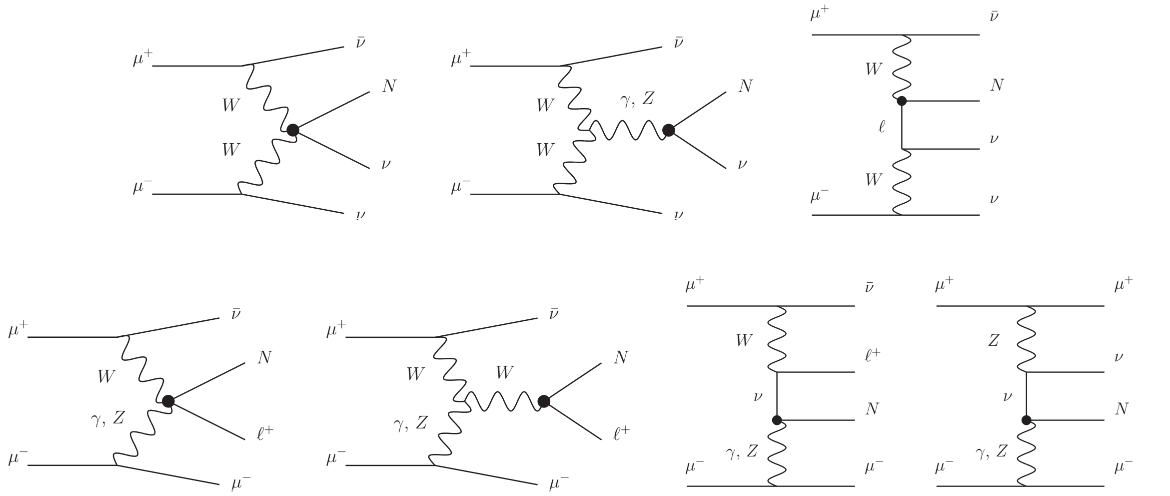

Figure 14. Representative Feynman diagrams for the N production at a muon collider in *VBF 2-4 processes*. Upper diagrams: "neutral" channels $\mu^+\mu^- \to N\nu\nu_\mu\bar{\nu_\mu}$. Lower diagrams: "charged" channels $\mu^+\mu^- \to N\ell\mu\nu$. Note that the latter include $\mu^+\mu^- \to N\nu\mu^+\mu^-$ events (last diagram).

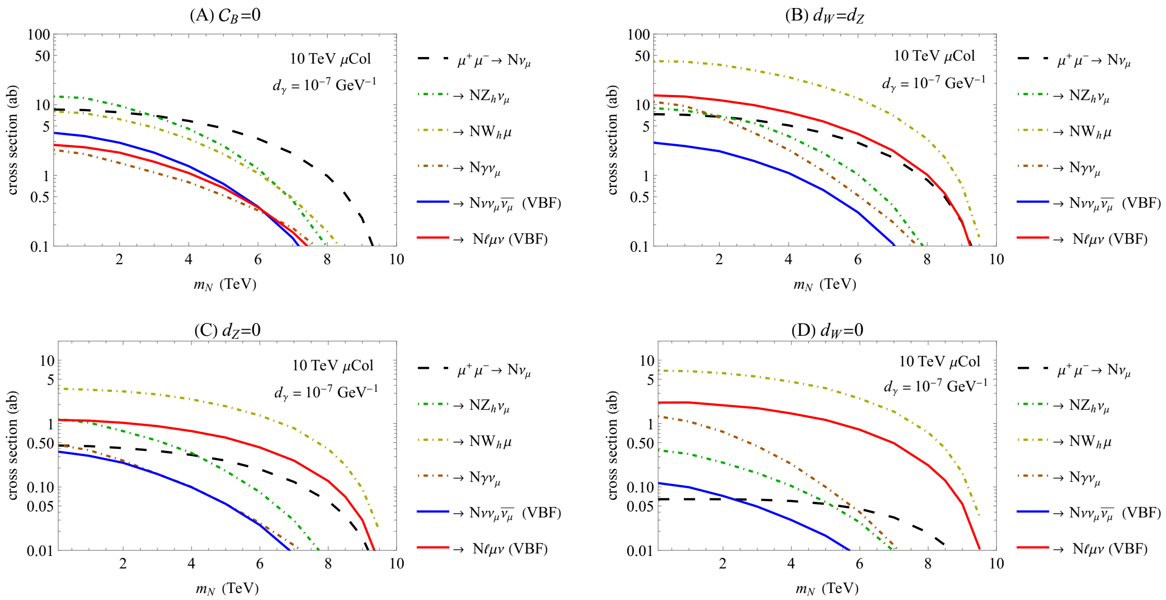

Figure 15. Cross section for the N production at a muon collider with $\sqrt{s} = 10\,\text{TeV}$ in the different theoretical benchmarks and channels: 2-2 process $\mu^+\mu^- \to N\nu$ (black-dashed curve), 2-3 processes $\mu^+\mu^- \to N\mu W_h$, $N\nu Z_h$, $N\nu\gamma$ (dot-dashed curves) and VBF 2-4 channels (continuous curves). Cross sections are shown for a reference value $d_\gamma = 10^{-7}\,\text{GeV}^{-1}$ as a function of the N mass.

Once again, a braided analysis in all available channels would be ideal. For the sake of concreteness, in the present study we will focus only on the most promising channels in each of the theoretical scenarios considered. Taking into account the cross section trends and branching ratios for the various benchmarks, we will analyze the channels (i) and (ii) for scenarios (A) and (B). Note that channel (ii) offers an opportunity (similarly to what we have already seen for hadronic colliders) to identify the flavor of the dipole operator involved in both the production[8] and the decay of the sterile neutrino. Due to the higher BRs in $\gamma\nu$ for the benchmarks (C) and (D), we will consider channel (iii). For channels (i) and (ii) involving a W, we will consider that it decays hadronically. As already highlighted in several previous studies [16, 17, 36], this W is highly boosted and can therefore be easily reconstructed as a single jet. For simplicity and similar to what was done in [16, 17], we will not include in our simulations the decay with subsequent hadronization and showering of the W, but we will take it into account by multiplying the signal and background yields by a factor $\mathrm{BR}(W \to jj) \approx 0.67$.

4.2 Search strategies and sensitivity projections in VBF channels

We outline signal selection strategies for the most promising channels, deriving sensitivity estimates of the muon collider to the sterile neutrino-dipole portal in the different benchmarks.

(i) $\mathbf{W_h^\pm \ell^\mp + E^{miss}}$

We focus on a final state consisting of exactly one lepton plus a hadronically decayed W and missing energy. This channel is particularly promising for the test of scenarios (A) $\mathcal{C}_B = 0$ and (B) $d_W = d_Z$. After imposing the acceptance requirements on the lepton and W_h transverse momenta and pseudo-rapidities: $p_T > 20\,\mathrm{GeV}$, $|\eta| < 2.5$, we find a total SM background at the level of 270 fb, dominantly given by $W_h \mu \nu_\mu$ events and subdominantly by $W_h W_\ell$ production. The latter, which includes both electrons and muons from the leptonic decay of W_ℓ has a cross section of about 4 fb. The signal is characterized by the hard emission of the lepton and the W_h and by large missing energy. We also observe that the signal lepton is emitted more centrally than in the background events. The sterile neutrino can be easily reconstructed by combining the lepton and the W_h. We thus apply the following signal selection cuts:

$$|\eta(\ell)| < 2\,,\; p_T \ell > 200\,\mathrm{GeV},\; E_T^{\mathrm{miss}} > 200\,\mathrm{GeV},\; p_T W_h > 200\,\mathrm{GeV},\; M_{W_h \ell} \in [0.8, 1.2] \cdot m_N\,,$$

which reduce the background cross section below $\sim$5 fb. We can refine the analysis for the case $N \to e W_h$. If we restrict ourselves to the electronic flavor, the background is in fact significantly lower (by approximately two orders of magnitude), receiving a contribution mainly from the subdominant background component $W_h(W \to e\nu_e)$. Applying the same selection cuts as in the generic flavor case, we therefore find higher sensitivities.

(ii) $\mathbf{W_h \ell\ell\mu + E^{miss}}$

In order to more efficiently probe the theoretical benchmarks (A) $\mathcal{C}_B = 0$ and (B) $d_W = d_Z$, we also focus on a final state consisting of a W_h, two leptons (emitted in the central region

[8] Except where N is produced in $\mu^+\mu^- \to N\nu\mu^+\mu^-$ channel from ZV scattering.

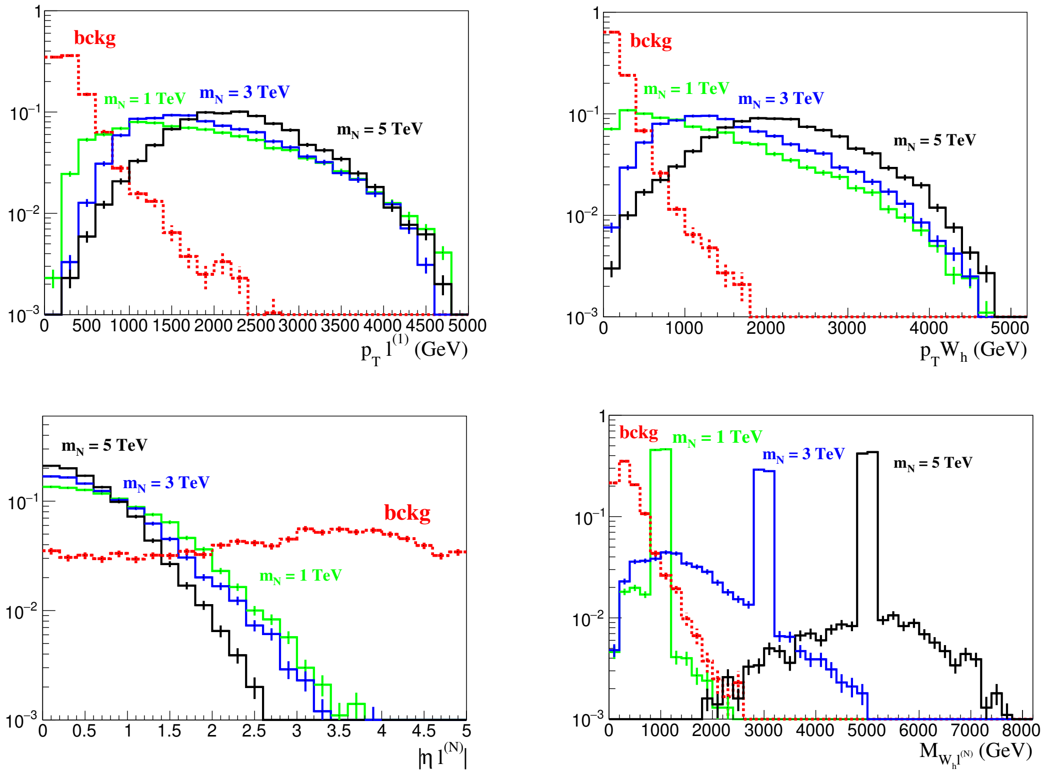

Figure 16. Distributions normalized to unit area for the $\mu^+\mu^- \to W_h \ell\ell\mu + E^{\rm miss}$ VBF dipole-portal signal (ii) in the benchmark (B) $d_W = d_Z$ (similar distributions are obtained in scenario (A)) with different N masses, and for the SM background. Upper plots: leading-p_T lepton (left) and W_h (right) transverse momentum distributions. Lower plots: pseudo-rapidity distribution of the identified lepton from N decay, $l^{(N)}$, (left) and invariant mass of the system consisting of $l^{(N)}$ and W_h (right plot).

$|\eta|$ <2.5 with a $p_T > 20\,$GeV), a muon (with rapidity up to $|\eta|$ <5 and $p_T > 20\,$GeV) and missing energy ($E_T^{\rm miss} > 20\,$GeV). The SM background, which includes $W_h W_\ell V_\ell$ events, is at the level of 40 fb after acceptance requirements.

As shown in figure 16, signal (ii) is characterized by the presence of the two leptons associated with the production and decay of N emitted at high p_T, together with W_h, and generally in the central region of the detector. The sterile neutrino can be quite efficiently reconstructed starting from W_h and identifying the lepton coming from its decay in the following way: for the less massive cases, $m_N < 5\,$TeV, this lepton, which we denote with $\ell^{(N)}$, is for the majority of signal events the one with the smallest separation ΔR from W_h. For cases $m_N \geq 5\,$TeV, $l^{(N)}$ instead coincides for the majority of signal events with the leading-p_T lepton $\ell^{(1)}$. We therefore apply the following selection cuts:

$$|\eta(\ell^{(N)})| < 2.5\,, \quad p_T\ell^{(1)} > 200\,\text{GeV}, \quad p_T W_h > 200\,\text{GeV}, \quad M_{W_h\ell^{(N)}} \in [0.8, 1.2]\cdot m_N\,.$$

After these cuts, the background is reduced to less than ∼1 fb.

(iii) $\gamma\ell\mu + \mathbf{E}^{\rm miss}$

We consider channel (iii) to better probe scenarios (C) and (D). In the final state, we require a photon (with $p_T > 20\,$GeV and $|\eta|$ <2.5), two leptons, one of which with muonic flavor

JHEP10(2025)125

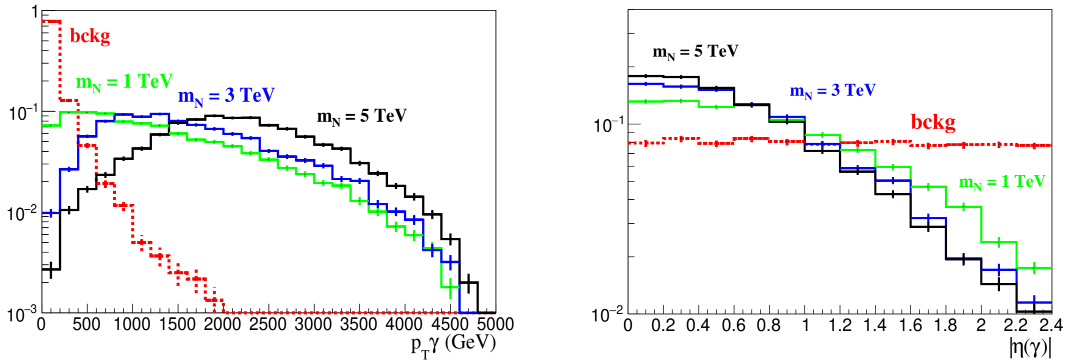

Figure 17. Distributions normalized to unit area for the $\mu^+\mu^- \to \gamma \ell \mu + E^{\rm miss}$ VBF dipole-portal signal (iii) in the benchmark (D) $d_W = 0$ (similar distributions are obtained in scenario (C)) with different N masses, and for the SM background. We plot the photon transverse momentum (left) and pseudorapidity (right) distributions.

(with $p_T > 20\,\text{GeV}$ and $|\eta| < 5$) and a large missing energy ($E_T^{\rm miss} > 20\,\text{GeV}$). The leptons must be separated from each other and from the photon by a distance $\Delta R > 0.4$. The dominant background consists of the SM production $\gamma \ell \mu \nu \bar{\nu}$, which includes contributions from $\gamma W_\ell^+ W_\ell^-$ and $\gamma Z_\ell (Z \to \nu \bar{\nu})$ events. After acceptance requirements, the background cross section is about 40 fb. The main features of the neutrino dipole-portal signal are the large missing energy and the very energetic photon, emitted much more centrally than the background, as we show in figure 17. We select the signal by applying the following cuts:

$$|\eta(\gamma)| < 1.5\,, \quad p_T\gamma > 20\% \cdot m_N, \quad E_T^{\rm miss} > 20\% \cdot m_N.$$

After these cuts, the background is reduced to less than $\sim$4 fb.

Our analyses in the various channels predict the 2σ sensitivities of the 10 TeV muon collider to the d_γ dipole operator shown in figure 18 for the different theoretical benchmarks (A)-(D). Note that the projected sensitivities refer equally to a muonic or electronic flavor (recall that we assumed a flavor-universal scenario). Sensitivity to flavors other than muonic is gained by taking advantage of the unique flavor-independent property of VBF production. Again, the shaded regions indicate a parameter space where the effective field theory description loses its validity. In scenario (A) $\mathcal{C}_B = 0$, in particular from the analysis of channel (i), sensitivities in the range $\sim$2-5$\times10^{-7}\,\text{GeV}^{-1}$ are obtained for N up to about 5 TeV. Channel (ii) is especially efficient for probing scenario (B) $d_W = d_Z$, reaching sensitivities of approximately 2.5-5 $\times10^{-7}\,\text{GeV}^{-1}$ for N up to $\sim$7 TeV. Scenarios (C) $d_Z = 0$ and (D) $d_W = 0$ can be efficiently tested in channel (iii), with sensitivities in the ranges $\sim$5.5-9$\times10^{-7}\,\text{GeV}^{-1}$ and $\sim$4-6$\times10^{-7}\,\text{GeV}^{-1}$ respectively for masses of N up to $\sim$9 and $\sim$8 TeV.

5 Results and outlook

In this work, we have explored novel strategies to probe a neutrino dipole portal at the energy frontier, focusing on the sterile neutrino production and decay signatures across a variety of future collider scenarios. We considered hadron colliders: the upcoming LHC high-luminosity program and the FCC-hh, and a futuristic muon collider at 10 TeV.

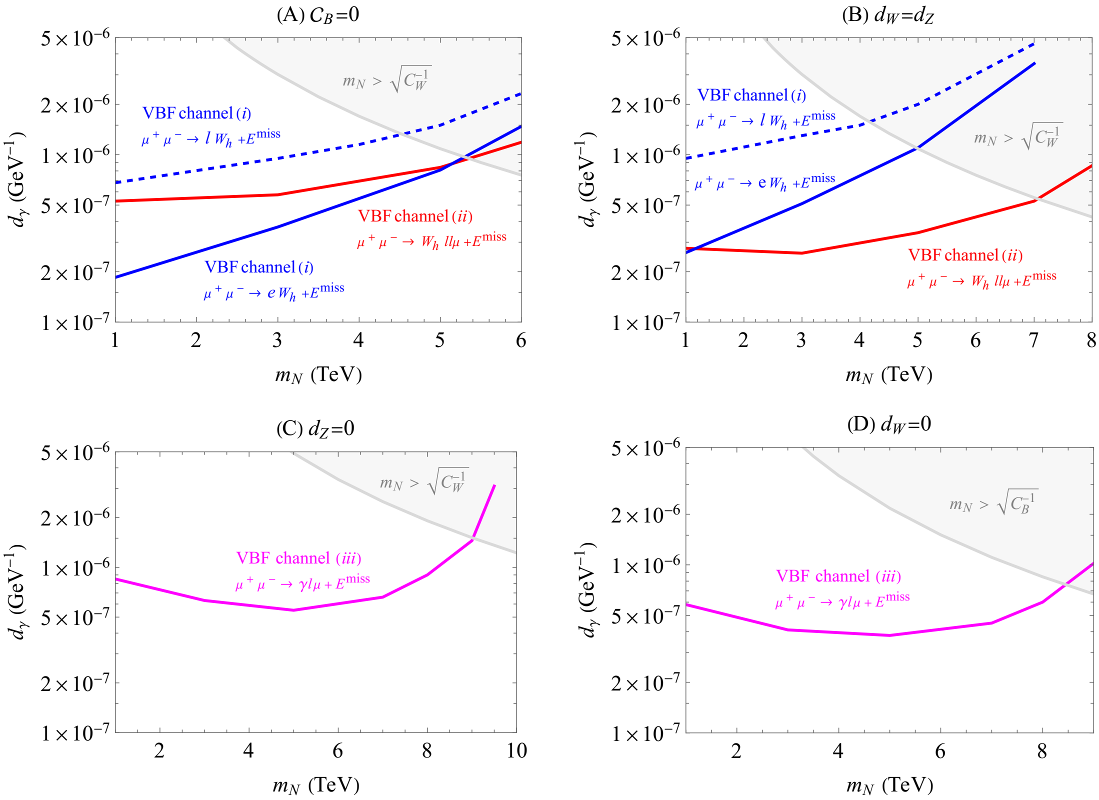

Figure 18. 2σ sensitivities of the 10 TeV muon collider to the dipole operator d_γ for the various theoretical benchmarks and in the different analyzed channels.

Our dedicated analysis for the High-Luminosity LHC demonstrated that in theoretical scenarios where the neutrino dipole is significantly generated by the $\mathrm{SU}(2)_w$ invariant operator $\mathcal{O}_W$, sensitivity to the dipole portal can be significantly improved by considering sterile neutrino decays in $W\ell$, leading to clean same-sign dilepton final states, in the case of Majorana nature of the sterile neutrino. As shown in figure 6, 2σ sensitivities to dipole couplings down to $d_\gamma \sim 3 \times 10^{-6}$ GeV^{-1} can be achieved, with flavor tagging offering potential insight into the operator structure.

At high energies probed by colliders such as FCC-hh and a muon collider, sterile neutrino production from gauge-boson scattering (VBF) becomes very significant and generally dominant. For the correct gauge-invariant treatment of these (and other) processes,[9] it is essential to include effective interactions with two gauge bosons, arising from the non-abelian operator $\mathcal{O}_W$. VBF channels, for which we identified different analysis strategies, can explore regions that are not accessible to other experiments so far.

At the FCC-hh, our results (figure 11) indicate that these channels, particularly the VBF-induced same-sign dilepton and $\ell\gamma jj$ final states, yield improved sensitivities up to $d_\gamma \sim 6 \times 10^{-7}$ GeV^{-1} for masses as large as 6 TeV in benchmarks with larger C_W values.

[9]Other important processes which require the inclusion of all the terms arising from $\mathcal{O}_W$ for a correct gauge-invariant treatment (unless in scenario $d_W = 0$) are represented by the 2-3 scatterings at a muon collider. In particular, the production channel $\mu^+\mu^- \to NW\mu$ shows a promising cross-section yield.

JHEP10(2025)125

Sensitivities are good anyway, $d_\gamma \sim 4\times10^{-6}\,\text{GeV}^{-1}$ up to about $m_N \sim 3.5\,\text{TeV}$, even in the case where the dipole is instead completely generated by the hypercharge-invariant operator $\mathcal{O}_B$. This extends the sensitivity frontier significantly beyond previous projections, which focused primarily on s-channel production and photon decays.

Most remarkably, our study of the 10 TeV muon collider shows that VBF processes provide access to sterile neutrino production even for non-muonic flavors — a critical point overlooked in previous literature. The muon collider achieves the highest sensitivity among all scenarios analyzed, reaching $d_\gamma \sim 2 \times 10^{-7}$ GeV^{-1} for the benchmarks with larger $\mathcal{C}_W$ values and remaining at sensitivities of the order $d_\gamma \lesssim 5\times10^{-7}\,\text{GeV}^{-1}$ for all the different theoretical benchmarks considered, as depicted in figure 18.

In summary, our results highlight the necessity of a fully gauge-invariant treatment of the neutrino dipole portal, including multi-boson operators, to accurately estimate sterile neutrino production at future colliders. Our findings open new directions for the experimental exploration of neutrino portals and demonstrate the significant potential of VBF channels to uncover physics beyond the Standard Model in the neutrino sector.

Acknowledgments

The author thanks Daniele Barducci for useful discussions and Vedran Brdar for clarifications regarding the study [17]. This work is supported by ICSC — Centro Nazionale di Ricerca in High Performance Computing, Big Data and Quantum Computing, funded by European Union — NextGenerationEU, reference code CN_00000013. This study also enjoyed enlightening discussions during the GGI workshop “Exploring the Energy Frontier with Muon Beams”.

Data Availability Statement. This article has no associated data or the data will not be deposited.

Code Availability Statement. This article has no associated code or the code will not be deposited.

References

[1] P. Minkowski, *$\mu \to e\gamma$ at a Rate of One Out of 10^9 Muon Decays?*, *Phys. Lett. B* **67** (1977) 421 [INSPIRE].

[2] M. Gell-Mann, P. Ramond and R. Slansky, *Complex Spinors and Unified Theories*, *Conf. Proc. C* **790927** (1979) 315 [arXiv:1306.4669] [INSPIRE].

[3] T. Yanagida, *Horizontal gauge symmetry and masses of neutrinos*, *Conf. Proc. C* **7902131** (1979) 95 [INSPIRE].

[4] R.N. Mohapatra and G. Senjanovic, *Neutrino Mass and Spontaneous Parity Nonconservation*, *Phys. Rev. Lett.* **44** (1980) 912 [INSPIRE].

[5] M. Fukugita and T. Yanagida, *Baryogenesis Without Grand Unification*, *Phys. Lett. B* **174** (1986) 45 [INSPIRE].

[6] E.K. Akhmedov, V.A. Rubakov and A.Y. Smirnov, *Baryogenesis via neutrino oscillations*, *Phys. Rev. Lett.* **81** (1998) 1359 [hep-ph/9803255] [INSPIRE].

[7] E. Bertuzzo and M. Frigerio, *Two portals to GeV sterile neutrinos: Dipole versus mixing*, *SciPost Phys.* **18** (2025) 140 [arXiv:2412.10101] [INSPIRE].

[8] V. Brdar, A. Greljo, J. Kopp and T. Opferkuch, *The Neutrino Magnetic Moment Portal: Cosmology, Astrophysics, and Direct Detection*, *JCAP* **01** (2021) 039 [arXiv:2007.15563] [INSPIRE].

[9] G. Magill, R. Plestid, M. Pospelov and Y.-D. Tsai, *Dipole Portal to Heavy Neutral Leptons*, *Phys. Rev. D* **98** (2018) 115015 [arXiv:1803.03262] [INSPIRE].

[10] F. Delgado et al., *Assessment of the dimension-5 seesaw portal and impact of exotic Higgs decays on non-pointing photon searches*, *JHEP* **09** (2022) 079 [arXiv:2205.13550] [INSPIRE].

[11] Y. Zhang and W. Liu, *Probing active-sterile neutrino transition magnetic moments at LEP and CEPC*, *Phys. Rev. D* **107** (2023) 095031 [arXiv:2301.06050] [INSPIRE].

[12] K. Jodłowski and S. Trojanowski, *Neutrino beam-dump experiment with FASER at the LHC*, *JHEP* **05** (2021) 191 [arXiv:2011.04751] [INSPIRE].

[13] L. Duarte, J. Jones-Pérez and C. Manrique-Chavil, *Bounding the Dimension-5 Seesaw Portal with non-pointing photon searches*, *JHEP* **04** (2024) 133 [arXiv:2311.17989] [INSPIRE].

[14] M. Ovchynnikov and J.-Y. Zhu, *Search for the dipole portal of heavy neutral leptons at future colliders*, *JHEP* **07** (2023) 039 [arXiv:2301.08592] [INSPIRE].

[15] R. Beltrán et al., *Probing heavy neutrino magnetic moments at the LHC using long-lived particle searches*, *JHEP* **07** (2024) 153 [arXiv:2405.08877] [INSPIRE].

[16] D. Barducci and A. Dondarini, *Neutrino dipole portal at a high energy $\mu-$collider*, *JHEP* **10** (2024) 165 [arXiv:2404.09609] [INSPIRE].

[17] V. Brdar, Y.-Y. Li, S.R. Mir and Y.-L. Wang, *Collider Prospects for the Neutrino Magnetic Moment Portal*, arXiv:2502.07024 [INSPIRE].

[18] FCC collaboration, *Future Circular Collider Feasibility Study Report: Volume 1, Physics, Experiments, Detectors*, arXiv:2505.00272 [DOI:10.17181/CERN.9DKX.TDH9] [INSPIRE].

[19] FCC collaboration, *FCC Physics Opportunities: Future Circular Collider Conceptual Design Report Volume 1*, *Eur. Phys. J. C* **79** (2019) 474 [INSPIRE].

[20] C. Accettura et al., *Towards a muon collider*, *Eur. Phys. J. C* **83** (2023) 864 [*Erratum ibid.* **84** (2024) 36] [arXiv:2303.08533] [INSPIRE].

[21] FCC collaboration, *FCC-hh: The Hadron Collider: Future Circular Collider Conceptual Design Report Volume 3*, *Eur. Phys. J. ST* **228** (2019) 755 [INSPIRE].

[22] M. Frigerio and N. Vignaroli, *Muon collider probes of Majorana neutrino dipole moments and masses*, *JHEP* **04** (2025) 008 [arXiv:2409.02721] [INSPIRE].

[23] P. Dehghani, M. Frank and B. Fuks, *Vector boson fusion signatures of superheavy Majorana neutrinos at muon colliders*, *Phys. Rev. D* **112** (2025) 035020 [arXiv:2506.06159] [INSPIRE].

[24] S. Balaji, M. Ramirez-Quezada and Y.-L. Zhou, *CP violation in neutral lepton transition dipole moment*, *JHEP* **12** (2020) 090 [arXiv:2008.12795] [INSPIRE].

JHEP10(2025)125

[25] J. Alwall et al., *The automated computation of tree-level and next-to-leading order differential cross sections, and their matching to parton shower simulations*, *JHEP* **07** (2014) 079 [arXiv:1405.0301] [INSPIRE].

[26] A. Alloul et al., *FeynRules 2.0 — A complete toolbox for tree-level phenomenology*, *Comput. Phys. Commun.* **185** (2014) 2250 [arXiv:1310.1921] [INSPIRE].

[27] C. Bierlich et al., *A comprehensive guide to the physics and usage of PYTHIA 8.3*, *SciPost Phys. Codeb.* **2022** (2022) 8 [arXiv:2203.11601] [INSPIRE].

[28] M. Cacciari, G.P. Salam and G. Soyez, *FastJet User Manual*, *Eur. Phys. J. C* **72** (2012) 1896 [arXiv:1111.6097] [INSPIRE].

[29] DELPHES 3 collaboration, *DELPHES 3, A modular framework for fast simulation of a generic collider experiment*, *JHEP* **02** (2014) 057 [arXiv:1307.6346] [INSPIRE].

[30] ATLAS collaboration, *Electron reconstruction and identification in the ATLAS experiment using the 2015 and 2016 LHC proton-proton collision data at* $\sqrt{s} = 13$ *TeV*, *Eur. Phys. J. C* **79** (2019) 639 [arXiv:1902.04655] [INSPIRE].

[31] K. Mohan and N. Vignaroli, *Vector resonances in weak-boson-fusion at future pp colliders*, *JHEP* **10** (2015) 031 [arXiv:1507.03940] [INSPIRE].

[32] D. Goncalves, T. Plehn and J.M. Thompson, *Weak boson fusion at 100 TeV*, *Phys. Rev. D* **95** (2017) 095011 [arXiv:1702.05098] [INSPIRE].

[33] M.J. Baker, T. Martonhelyi, A. Thamm and R. Torre, *The role of vector boson fusion in the production of heavy vector triplets at the LHC and HL-LHC*, *JHEP* **11** (2022) 066 [arXiv:2207.05091] [INSPIRE].

[34] E. Molinaro, F. Sannino, A.E. Thomsen and N. Vignaroli, *Uncovering new strong dynamics via topological interactions at the 100 TeV collider*, *Phys. Rev. D* **96** (2017) 075040 [arXiv:1706.04037] [INSPIRE].

[35] A. Costantini et al., *Vector boson fusion at multi-TeV muon colliders*, *JHEP* **09** (2020) 080 [arXiv:2005.10289] [INSPIRE].

[36] N. Vignaroli, *Charged resonances and MDM bound states at a multi-TeV muon collider*, *JHEP* **10** (2023) 121 [arXiv:2304.12362] [INSPIRE].

JHEP10(2025)125